

# Global and Unified Analysis of Solar Neutrino Data

M.C. Gonzalez-Garcia and C. Peña-Garay <sup>a,\*</sup>

<sup>a</sup>Instituto de Física Corpuscular  
 Universitat de València – C.S.I.C  
 Edificio Institutos de Paterna, Apt 2085, 46071 València, Spain

We discuss the status of the solutions of the solar neutrino problem in terms of oscillations of  $\nu_e$  into active or sterile neutrinos. We present the results of a global fit to the full data set corresponding to the latest Super-Kamiokande (SK) data on the total event rate, their day–night dependence and the recoil electron energy spectrum, together with the data from Chlorine and Gallium experiments presented at the  $\nu$ -2000 conference. We show the possible solutions in the full parameter space for oscillations including both MSW and vacuum, as well as quasi-vacuum oscillations (QVO) and matter effects for mixing angles in the second octant (the so called dark side). We quantify our results in terms of allowed regions as well as the goodness of the fit (GOF) for the different allowed solutions. Our conclusion is that from the statistical point of view, all solutions for oscillations into active neutrinos: the large mixing angle (LMA), the low mass (LOW), the small mixing angle (SMA) and the QVO solutions are acceptable since they all provide a reasonable GOF to the full data set. The same holds for the SMA solution for oscillations into sterile neutrinos. LMA and LOW-QVO solutions for oscillations into active neutrinos seem slightly favoured over SMA solutions for oscillations into active or sterile neutrinos but these last two are not ruled out. We also analyze the dependence of these conclusions on the uncertainty of the SSM  $^8\text{B}$  flux and on the removal of the data from one of the experimental rates. We also present the results in the framework of four neutrino oscillations which allows for oscillations into a state which is a combination of active and sterile neutrino.

## 1. Introduction: Experimental Status

The sun is a source of  $\nu_e$ 's which are produced in the different nuclear reactions taking place in its interior. Along this talk we will use the  $\nu_e$  fluxes from Bahcall–Pinsonneault calculations [1] which we refer to as the solar standard model (SSM).

At present these neutrinos have been detected at the Earth by seven experiments which use different detection techniques:

- Homestake (chlorine) [2]  $\nu_e + ^{37}\text{Cl} \rightarrow ^{37}\text{Ar} + e^-$
- SAGE [3] and GALLEX+GNO [4,5] (gallium)  $\nu_e + ^{71}\text{Ga} \rightarrow ^{71}\text{Ge} + e^-$
- Kamiokande and SK [6,7]  $\nu_e e$  scattering on water

Due to the different energy threshold for the detection reactions, these experiments are sensitive

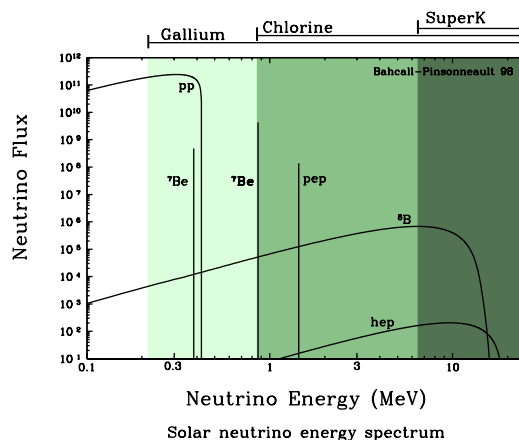


Figure 1. Bahcall–Pinsonneault solar neutrino fluxes.

\*Expanded version of the proceedings for the talk presented at  $\nu$ -2000 Conference, Sudbury, Canada, June 2000. This work was supported by the spanish DGICYT grants PB98-0693 and PB97-1261, by the Generalitat Valenciana grant GV99-3-1-01 and by the TMR EU network grant ERBFMRXCT960090.

to different parts of the solar neutrino spectrum as represented in Fig. 1. They all observe a deficit between 30 and 60 % which seems to be energy dependent mainly due to the lower Chlorine rate.

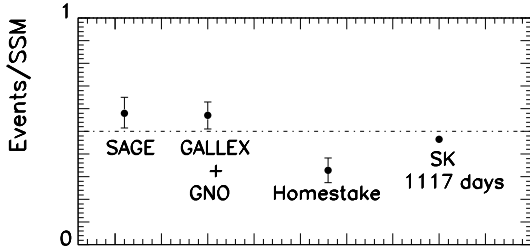


Figure 2. Measured solar neutrino event rates normalized to the SSM prediction.

To the measurements of these six experiments we have to add also the new results from SNO [8] first presented in this conference. They are however still not in the form of definite measured rates which could be included in this analysis.

In this conference SK has also presented their results after 1117 days of data taking on:

- The recoil electron energy spectrum: SK has measured the dependence of the even rates on the recoil electron energy spectrum divided in 18 bins starting at 5.5 MeV. They have also reported the results of a lower energy bin  $5 \text{ MeV} < E_e < 5.5 \text{ MeV}$ , but its systematic errors are still under study and it is not included in their nor our analysis. The spectrum shows no clear distortion with  $\chi^2_{flat} = 13/(17dof)$ . 17 dof=18 bins-1 free normalization.

- The zenith Angle Distribution (Day/Night Effect) which measures the effect of the Earth Matter in the neutrino propagation. We have included in the analysis the experimental results from SK on the zenith angle distribution of events taken on 5 night periods and the day averaged value. SK finds few more events at night than during the day but the corresponding Day-Night asymmetry

$$A_{D/N} = \frac{D - N}{\frac{D+N}{2}} = -0.034 \pm 0.022 \pm 0.013 \quad (1)$$

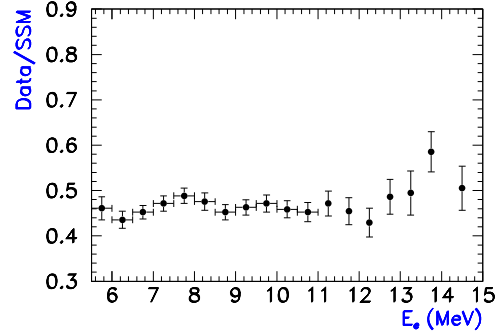


Figure 3. Recoil electron energy spectrum measured by SK normalized to the SSM prediction.

is only  $1.3\sigma$  away from zero.

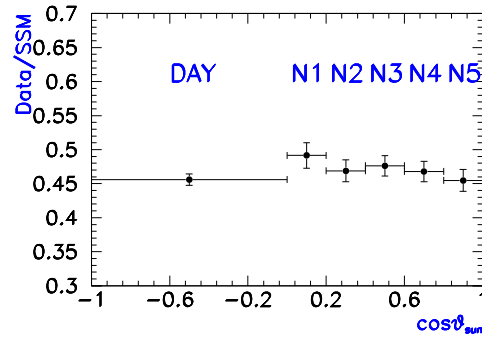


Figure 4. Zenith angle distribution measured by SK normalized to the SSM prediction.

In order to combine both the Day-Night information and the spectral data SK has also presented separately the measured recoil energy spectrum during the day and during the night. This will be referred in the following as the day-night spectra data which contains  $2 \times 18$  data bins.

The most generic and popular explanation of the solar neutrino anomaly is in terms of neutrino masses and mixing leading to oscillations of  $\nu_e$  into an active ( $\nu_\mu$  and/or  $\nu_\tau$ ) or sterile neutrino,  $\nu_s$ . We pass now to discuss some issues that have been raised lately in the literature concerning the computation of the corresponding neutrino sur-

vival probabilities in the full range of mass and mixing relevant to the solar neutrino problem.

## 2. Survival Probabilities: QVO and the Dark side

The presence of neutrino mass and mixing imply the possibility of neutrino oscillations. For solar neutrinos we know that depending on the range of mass and mixing  $\nu_e$  can undergo oscillations either in *vacuum* [9] or via the matter-enhanced *MSW mechanism* [10]. However this *broken* picture of solar neutrino oscillations contains a set of approximations which, as we discuss next, are not longer phenomenologically valid when performing the analysis of the solar neutrino data. In order to clarify this issue let us first review the calculation of the solar neutrino survival probability in the two-neutrino mixing case.

The survival amplitude for a solar  $\nu_e$  neutrino of energy  $E$  at a detector in the Earth can be written as:

$$A_{ee} = \sum_{i=1}^2 A_{ei}^S A_{ie}^E \exp[-im_i^2(L-r)/2E]. \quad (2)$$

Here  $A_{ei}^S$  is the amplitude of the transition  $\nu_e \rightarrow \nu_i$  ( $\nu_i$  is the  $i$ -mass eigenstate) from the production point to the Sun surface,  $A_{ie}^E$  is the amplitude of the transition  $\nu_i \rightarrow \nu_e$  from the Earth surface to the detector, and the propagation in vacuum from the Sun to the surface of the Earth is given by the exponential.  $L$  is the distance between the center of the Sun and the surface of the Earth, and  $r$  is the distance between the neutrino production point and the surface of the Sun. The corresponding survival probability  $P_{ee}$  is then given by:

$$P_{ee} = P_1 P_{1e} + P_2 P_{2e} + 2\sqrt{P_1 P_2 P_{1e} P_{2e}} \cos \xi \quad (3)$$

Here  $P_i \equiv |A_{ei}^S|^2$  is the probability that the solar neutrinos reach the surface of the Sun as  $|\nu_i\rangle$ , while  $P_{ie} \equiv |A_{ie}^E|^2$  is the probability of  $\nu_i$  arriving at the surface of the Earth to be detected as a  $\nu_e$ . Unitarity implies  $P_1 + P_2 = 1$  and  $P_{1e} + P_{2e} = 1$ . The phase  $\xi$  is given by

$$\xi = \frac{\Delta m^2(L-r)}{2E} + \delta, \quad (4)$$

where  $\delta$  contains the phases due to propagation in the Sun and in the Earth and can be safely neglected. In the evaluation of both  $P_1$  and  $P_{2e}$  the effect of coherent forward interaction with the Sun and Earth matter must be taken into account.

From Eq. (3) one can recover more familiar expressions for  $P_{ee}$ :

(1) For  $\Delta m^2/E \lesssim 5 \times 10^{-17}$  eV, the matter effect suppresses flavour transitions both in the Sun and the Earth. Consequently, the probabilities  $P_1$  and  $P_{2e}$  are simply the projections of the  $\nu_e$  state onto the mass eigenstates:  $P_1 = \cos^2 \theta$ ,  $P_{2e} = \sin^2 \theta$ . In this case we are left with the standard vacuum oscillation formula:

$$P_{ee}^{vac} = 1 - \sin^2 2\theta \sin^2(\Delta m^2(L-r)/4E) \quad (5)$$

which describes the oscillations on the way from the surface of the Sun to the surface of the Earth. The probability is symmetric under the change of octant  $\theta \leftrightarrow \frac{\pi}{2} - \theta$  and change of mass sign  $\Delta m^2 \leftrightarrow -\Delta m^2$ . Notice that the simultaneous application of both symmetries translates simply into a relabelling of the mass eigenstates  $\nu_1 \leftrightarrow \nu_2$ . Therefore only one of these symmetries is physically independent. This means that we can take  $\Delta m^2 > 0$  without loss of generality and keep  $0 < \theta < \frac{\pi}{2}$ . Then the symmetry of the survival probability under the change of octant  $\theta \leftrightarrow \frac{\pi}{2} - \theta$  implies that each point in the  $(\Delta m^2, \sin^2(2\theta))$  parameter space corresponds to two physically independent solutions one in each octant.

Averaging Eq.(5) over the Earth Orbit  $L(t) = L_0[1 - \varepsilon \cos 2\pi \frac{t}{T}]$  one gets :

$$\langle P_{ee}^{vac} \rangle = 1 - \frac{1}{2} \sin^2 2\theta \left[ 1 - \cos\left(\frac{\Delta m^2 L_0}{2E}\right) J_0\left(A = \frac{\varepsilon \Delta m^2 L_0}{2E}\right) \right] \quad (6)$$

where  $\varepsilon = 0.0167$  is the orbit eccentricity and  $J_0$  is the Bessel function. In Fig. 5.a we display the value of  $\langle P_{ee}^{vac} \rangle$  as a function of  $4E/\Delta m^2$ . As seen in the figure for large values of  $\Delta m^2$  the probability averages out to a constant value  $1 - \frac{1}{2} \sin^2(2\theta)$ .

(2) For  $\Delta m^2/E \gtrsim 10^{-14}$  eV, the last term in Eq. (3) vanishes and we recover the incoherent MSW survival probability. In this case  $P_1$  and  $P_{2e}$  must be obtained by solving the evolution

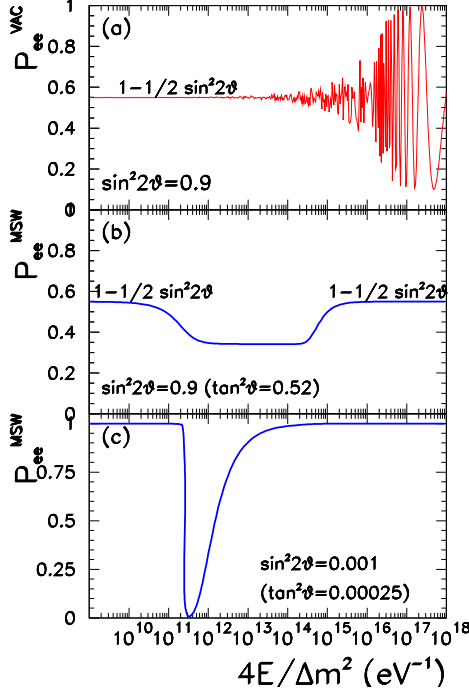


Figure 5.  $P_{ee}$  as a function of  $4E/\Delta m^2$ .

equation of the neutrino states in the Sun and the Earth matter respectively:

$$-i \frac{d}{dt} \begin{pmatrix} \nu_e \\ \nu_X \end{pmatrix} = \begin{pmatrix} V_e + \frac{\Delta m^2}{2E} \cos 2\theta & -\frac{\Delta m^2}{2E} \sin 2\theta \\ -\frac{\Delta m^2}{2E} \sin 2\theta & V_X - \frac{\Delta m^2}{2E} \cos 2\theta \end{pmatrix} \begin{pmatrix} \nu_e \\ \nu_X \end{pmatrix} \quad (7)$$

with

$$V_e = \frac{\sqrt{2}G_F}{M}(N_e - \frac{1}{2}N_n) \quad V_s = 0$$

$$V_\mu = V_\tau = \frac{\sqrt{2}G_F}{M}(-\frac{1}{2}N_n) \quad (8)$$

where  $N_{e(n)}(r)$  is the electron (nucleon) number density which are proportional to the Sun or Earth matter density. In Fig. 6 we show  $N_e(r)$  for the Sun. As seen in the figure the Sun density profile for  $r < 0.9R_\odot$  can be very well approximated by an exponential  $N(r) = N_0 \exp(-r/r_0)$  with constant exponent slope  $r_0 = R_\odot/10.54$ .

The approximate solution for the evolution in

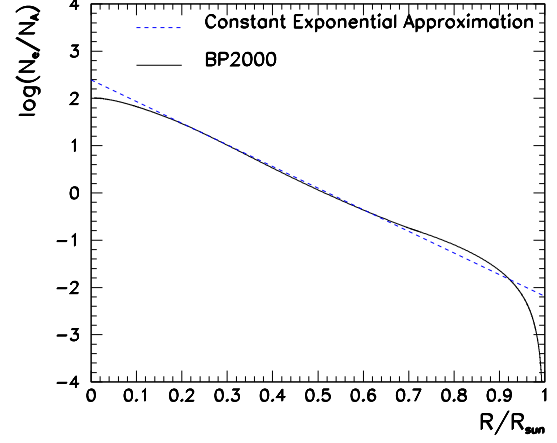


Figure 6. Solar density profile for BP2000 model.

the Sun takes the well-known form

$$P_1 = \frac{1}{2} + \left(\frac{1}{2} - P_c\right) \cos(2\theta_{m,0}) \quad (9)$$

where  $P_c$  denotes the standard Landau-Zener probability [11] and  $\theta_{m,0}$  is the mixing angle in matter at the neutrino production point:

$$\cos(2\theta_{m,0}) = \frac{\Delta m^2 c^2 - A_0}{\sqrt{(\Delta m^2 c^2 - A_0)^2 + (\Delta m^2 s^2)^2}} \quad (10)$$

$$P_c = \frac{\exp[-\gamma \sin^2 \theta] - \exp[-\gamma]}{1 - \exp[-\gamma]} \quad (11)$$

$$\gamma = \pi \frac{\Delta m^2}{E} \left[ \left| \frac{d \ln N_e(r)}{dr} \right|_{r=r_{res}} \right]^{-1}$$

with  $A_0 = 2E(V_e - V_X)$  evaluated at the production point,  $c^2 = \cos(2\theta)$  and  $s^2 = \sin(2\theta)$ . For the approximation of exponential density profile  $\gamma = \pi \frac{\Delta m^2}{E} r_0$  which is independent of the point in the Sun where the resonance takes place. Improvement over this ‘‘constant slope’’ exponential density profile approximation can be obtained by numerically deriving the exact  $N_e(r)$  profile at the resonant point. In this case  $\gamma = \pi \frac{\Delta m^2}{E} r_0(r_{res})$ .

The physical interpretation behind Eq.(9) is very simple. At the production point  $\nu_e$  has a projection over the mass eigenstate  $\nu_1$  given by the mixing angle in matter  $\theta_{m,0}$ . This neutrino evolves adiabatically till the resonant point where

both mass eigenvalues become closer and the neutrino has a probability  $P_c$  of "jumping" into the other mass eigenstate (or staying in the state  $\nu_1$  with a probability  $1-P_c$ ). During the day no Earth matter effect is to be included and the survival probabilities  $P_{ie}$  are obtained by simple projection of the  $\nu_e$  state onto the mass eigenstates  $P_{2e,DAY} = 1 - P_{1e,DAY} = \sin^2 \theta$  and one obtains

$$P_{ee,DAY}^{MSW} = \frac{1}{2} + \left(\frac{1}{2} - P_c\right) \cos(2\theta_{m,0}) \cos(2\theta) \quad (12)$$

In Fig. 5.b ( 5.c) we plot the this survival probability as a function of  $4E/\Delta m^2$  for large (small) mixing angle.

Let us make some remarks concerning Eq.(12):

(i) In both limits of very large and very small  $E/\Delta m^2$   $P_{ee}^{MSW} \rightarrow 1 - \frac{1}{2} \sin^2(2\theta)$  (See Fig.5.b). For large  $E/\Delta m^2$ ,  $P_c = \cos^2 \theta$  and  $\cos(2\theta_{m,0}) = -1$ . While for small  $E/\Delta m^2$ ,  $P_c = 0$  and  $\cos(2\theta_{m,0}) = \cos(2\theta)$ . So in principle one could expect a perfect connection between the asymptotic small  $E/m^2$  probability for the vacuum oscillation regime and the large  $E/m^2$  behaviour of the MSW regime. However as seen when comparing panels (a) and (b) of Fig.5 there is an intermediate range,  $2 \times 10^{14} \lesssim 4E/\Delta m^2 \lesssim 10^{16}$  eV, where both adiabaticity is violated and the  $\cos \xi$  coherent term should be taken into account. The result is similar to vacuum oscillations but with small matter corrections. We define this case as QVO [14–16]. The range of  $E/m^2$  for the QVO regime depends on the value of  $E/m^2$  for which the MSW probability in Eq. 12 acquires the asymptotic value  $1 - \frac{1}{2} \sin^2(2\theta)$ , the smaller  $E/m^2$  the more separated the MSW and vacuum regimes are, and the narrower the QVO region is.

(ii) Due to matter effects  $P_{ee}^{MSW}$  is only symmetric under simultaneous  $(\Delta m^2, \theta) \rightarrow (-\Delta m^2, \frac{\pi}{2} - \theta)$ . For  $\Delta m^2 > 0$  the resonance is only possible for  $\theta < \frac{\pi}{4}$  and MSW solutions are usually plotted in the  $(\Delta m^2, \sin^2(2\theta))$  plane assuming that now each point on this plane represents only one physical solution with  $\theta$  in the first octant. But in principle non-resonant solutions are also possible for  $\theta > \frac{\pi}{4}$ , the so called *dark side* [18–20,22].

It is clear from these considerations that in order to compute the survival probability for so-

lar neutrinos, valid for any value of the neutrino mass and mixing, the full expression (3) has to be evaluated. The results presented in the following sections have been obtained using the general expression for the survival probability in Eq. (3) with  $P_1$  and  $P_{2e}$  found by numerically solving the evolution equation in the Sun and the Earth matter. For  $P_1$  we use the electron number density of BP2000 model [12]. For  $P_{2e}$  we integrate numerically the evolution equation in the Earth matter using the Earth density profile given in the Preliminary Reference Earth Model (PREM) [13].

Before moving to the next section we want to discuss the validity of the analytical and semi-analytical approximations based on the exponential profile for the sun density in the evaluation of the survival probability when used to describe the matter effects in the QVO regime as well as for mixing angles in the second octant. In order to illustrate this point we display in Fig. 7 the survival probability  $P_{ee}$  (without the oscillating  $\cos \xi$  term) as a function of  $4E/\Delta m^2$  for different values of the mixing angle obtained by our numerical solution as well as from the corresponding analytical approximations (12). We discuss two analytical approximations: the exponential approximation with constant slope  $r_0 = R_\odot/1054$  and with point dependent slope  $r_0(r)$ .

We see from Fig. 7 that the analytical results differ from the results of the numerical calculations. In particular, the analytical result with constant exponential slope shows a "slower" transition to the vacuum oscillation regime or, in other words, it overestimates the size of the matter effects in the QVO region. The same value of the survival probability appears for about twice larger  $E/\Delta m^2$ . This is due to the fact that for such values of  $E/\Delta m^2$  the adiabaticity breaking occurs very close to the Sun edge where the density falls much faster than the exponential approximation as shown in Fig. 6. Similar conclusions have been drawn in Refs. [15–17]. On the other hand the analytical approximation with point dependent slope shows a "faster" transition to the vacuum oscillation regime or, in other words, it underestimates the size of the matter effects in the QVO region.

Notice also that, originally, Eq. (11) was de-

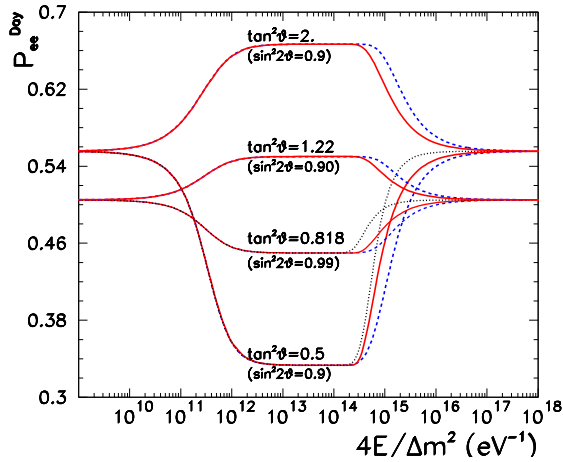


Figure 7. Survival probabilities as a function of  $4E/\Delta m^2$  for different values of the mixing angle. The full line corresponds to the numerical solution while the dashed (dotted) lines corresponds to the analytical approximation for exponential density profile with constant (point dependent) slope.

rived for a mixing angle  $\theta < \frac{\pi}{4}$  where resonant enhancement is possible. However for the constant slope exponential profile,  $\gamma$  is constant (independent of the resonant condition) and both Eq. (10) and Eq. (11) can be analytically continued into the second octant,  $\theta > \pi/4$ , and used to compute the corresponding survival probability. This is illustrated in Fig. 7. As seen in the figure, for values of the mixing angle close to maximal mixing  $\theta = \pi/4$ , the survival probability is mirror-symmetric in the first and second octant, while, as expected, the symmetry breaks down as we depart from maximal mixing. We also see that the analytical approximation overestimates the size of matter effects in the QVO region on the second octant as well.

Finally we want to comment briefly on the Earth matter effects. In Fig. 8 we show the Earth regeneration factor  $R_E = P_{2e,NIGHT} - P_{2e,DAY}$  (obtained numerically) as a function of  $4E/\Delta m^2$  for two values of the mixing angle in the first and second octant. We see that:

- (a) Earth Matter effects are only relevant in

the “pure” MSW regime  $4E/\Delta m^2 \lesssim 10^{-14} \text{ eV}^{-1}$ , while they are very small for QVO.

(b) Earth Regeneration is always positive (it always leads to an increase of the  $\nu$  flux at night) for mixing angles both in the first or in the second octant.

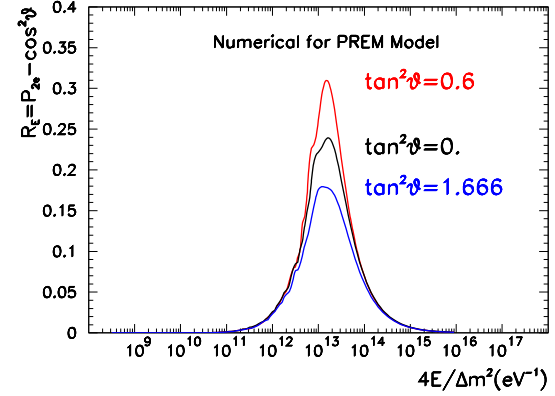


Figure 8. Regeneration of  $\nu_e$  in the Earth matter as a function of the  $4E/\Delta m^2$  for different mixing angles.

### 3. Two-neutrino Oscillations

We now describe the results of the analysis of the solar neutrino data in terms of  $\nu_e$  oscillations into active or sterile neutrinos. For details on the statistical analysis applied to the different observables we refer to Ref. [21].

We first determine the allowed range of oscillation parameters using only the total event rates of the Chlorine, Gallium and SK experiments shown in Fig.2. For the Gallium experiments we have used the weighted average of the results from GALLEX+GNO and SAGE detectors and we do not include the Kamiokande data as it is well in agreement with the results from the SK experiment and the precision of this last one is much higher.

Using the predicted fluxes from the BP98 model the  $\chi^2$  for the total event rates is  $\chi^2_{SSM} = 60$  for 3 d. o. f. This means that the SSM together with the SM of particle interactions can explain

the observed data with a probability lower than  $10^{-12}$ .

The allowed regions in the oscillation parameter space are shown in Fig. 9. In the case of active–active neutrino oscillations we find that the best–fit point is obtained for the SMA solution which has a probability or goodness of the fit of 50 the LMA and LOW solutions. In the region of vacuum oscillations we find a “tower” of regions around local minima corresponding to the oscillation wavelength being an entire fraction of the Sun–Earth distance. In Table 1 we give the values of the parameters in these minima as well as the GOF corresponding to each solution.

Notice that following the standard procedure, the allowed regions for a given set of observables are defined in terms of shifts of the  $\chi^2$  function for those observables *with respect to the global minimum in the plane*. Defined this way, the size of a region depends on the *relative* quality of its local minimum with respect to the global minimum but from the size of the region we cannot infer the actual *absolute* quality of the description in each region. In order to give this information we list in Table 1 the GOF for each solution obtained from the value of  $\chi^2$  at the different minima. We see that for oscillations into active neutrinos the best solution by far for the description of the rates is the SMA.

For oscillations into sterile neutrinos we find only the SMA solution and some small region for LOW–QVO. The LMA and most of the LOW solutions are not acceptable for oscillation into sterile neutrinos. Unlike active neutrinos which lead to events in the SK detector by interacting via neutral current (NC) with the electrons, sterile neutrinos do not contribute to the SK event rates. Therefore a larger survival probability for  $^8B$  neutrinos is needed to accommodate the measured rate. As a consequence a larger contribution from  $^8B$  neutrinos to the Chlorine and Gallium experiments is expected, so that the small measured rate in Chlorine can only be accommodated if no  $^7Be$  neutrinos are present in the flux. This is only possible in the SMA solution region, since in the LMA and LOW regions the suppression of  $^7Be$  neutrinos is not enough. Notice also the SMA region for oscillations into sterile neu-

trinos is slightly shifted downwards as compared with the active case. This is due to the small modification in the neutrino survival probability induced by the different matter potentials. The matter potential for sterile neutrinos is smaller than for active neutrinos due to the negative NC contribution proportional to the neutron abundance (see Eq. (8)). For this reason the resonant condition for sterile neutrinos is achieved at lower  $\Delta m^2$ .

On the other hand SK data on the day–night variation of the event rates and the spectrum data lead to excluded regions in the parameter space. Since both the observed zenith angular dependence and the recoiled energy spectrum are compatible with the no–oscillation hypothesis (up to an overall normalization which is taken free), these measurements translate in the exclusion of those regions of the oscillation parameter space where the expectation for those observables is far different from the no–oscillation one. In this way we see in Figs. 10, 11 and 12 the regions excluded by the zenith angle, average spectrum and combined day–night spectra data. The zenith angular data excludes the region where large regeneration in the Earth is expected (See Fig. 8) which for neutrino energies of few MeV (above SK threshold) occurs for few  $10^{-8} \lesssim \Delta m^2/\text{eV}^2 \lesssim 10^{-5}$ . In Table 1 we show the effect of the inclusion of this observation in the position of the different local minima. We see that when combined with the zenith angle data the LMA minimum is shifted up and the LOW minimum is shifted down towards values of parameters where the Earth regeneration is smaller.

The excluded region from the non observation of any clear distortion of the energy spectrum is shown in Fig. 11. Its main effect is to suppress the vacuum oscillation solution where a large distortion of the spectrum is expected due to the “imprints” of the oscillation wavelength. On the other hand for the SMA a positive tilt of the spectrum is also predicted due to the raising with the neutrino energy of the survival probability (see Fig. 5.c). For this reason the local SMA minimum shifts to lower values of the mixing angle where a flatter probability is expected. On the other hand both LMA and LOW solutions pre-

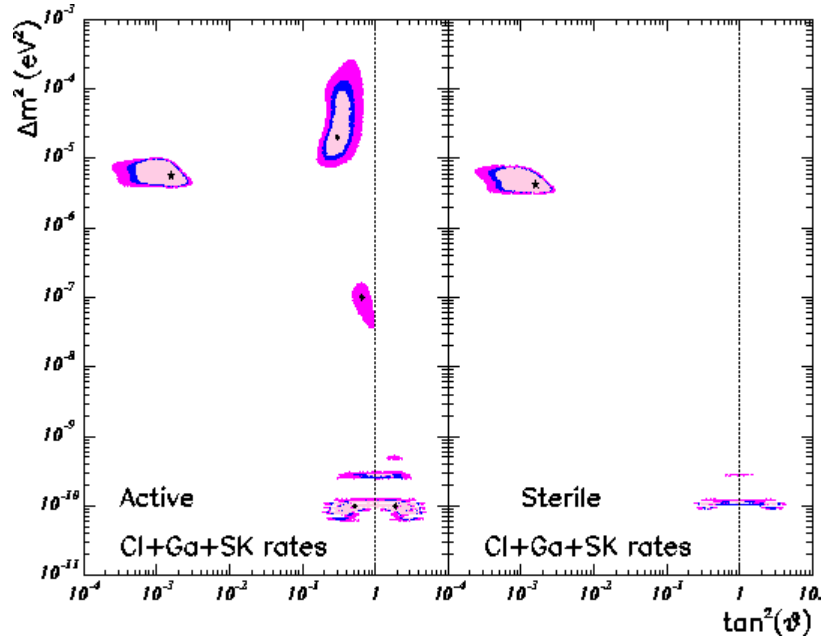


Figure 9. 90, 95 and 99 % CL allowed regions from the analysis of the total rates only. The global minimum is marked with a star while the local minima are denoted with a dot.

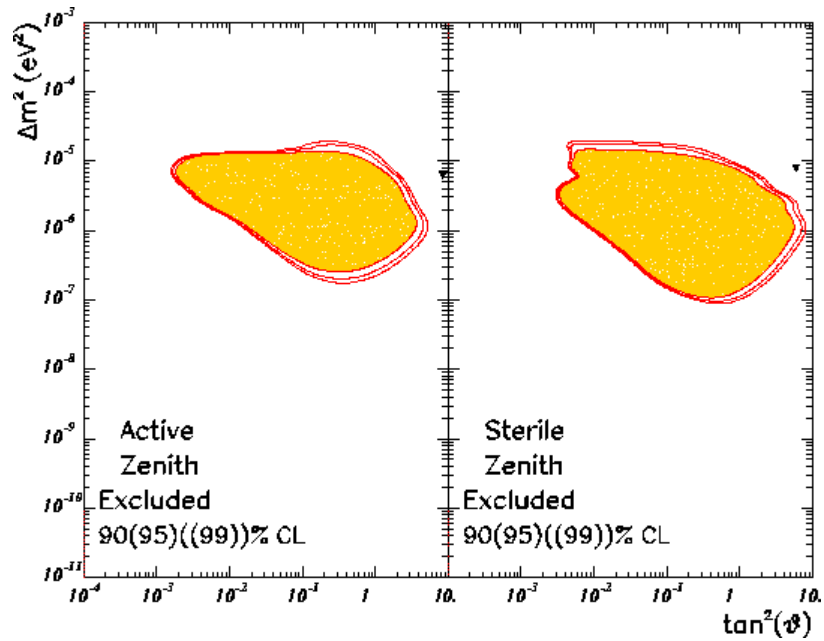


Figure 10. 99 (shadow), 95 and 90 excluded regions from the analysis of SK measured zenith angle dependence. The inverted triangle represents the minimum used to define the regions.



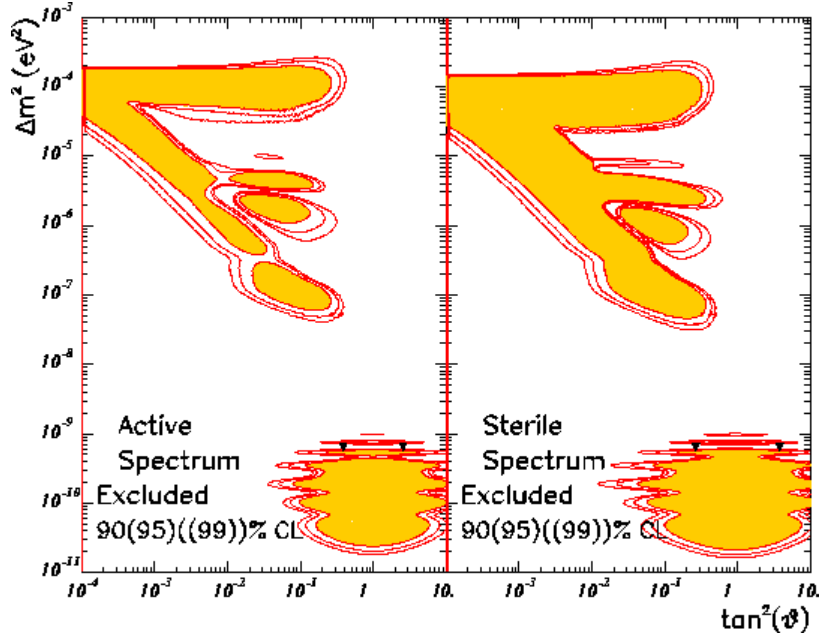


Figure 11. 99 (shadow), 95 and 90 excluded regions from the analysis of the dally averaged SK measured spectrum. The inverted triangle represents the minimum used to define the regions.

dict a rather flat spectrum and in consequence the position of these minima are little affected.

Finally Fig. 12 shows the excluded region from the SK day–night spectra which contains simultaneously the information on the Earth regeneration effect and the energy dependence of the survival probability. Combining statistically this information with the data from the total rates (what implies  $3+2 \times 18$  data points with 1 free normalization for the spectra) we obtain the allowed regions which we display in Fig. 13 while the corresponding GOF for the global solutions are given in Table 1. There are some points concerning these results that we would like to stress:

(a) Despite giving a worse fit to the observed total rates, once the day–night spectra data is included the LMA gives the best fit. This is mainly driven by the flatness of the spectrum and it was already the case with the last year data as pointed out in Ref. [21].

(b) The GOF of the LOW solution has increased considerably as it describes the spectrum data very well despite it gives a bad fit to the global rates. LOW and QVO regions are con-

nected at the 99 %CL and they extend into the second octant so maximal mixing is allowed at 99 % CL for  $\Delta m^2$  in the LOW-QVO region. Notice that part of this allowed region would be missing when making the *old fashioned* analysis in terms of pure MSW or vacuum oscillations.

(c) What is the situation for the SMA solution?. Superimposing the excluded region from the day–night spectra in Fig. 12 with the allowed region from the global rates in Fig. 9 we see that almost the full allowed region at 95 %CL lays below the 95% CL excluded region from the day–night spectra. However this does not mean that the SMA solution is ruled out at that CL. The result from the correct statistically combined analysis is what we show in Fig. 13 and more important in Table 1. From this results we learn that the SMA can describe the full data set with a probability of 34%, but it is now shifted to smaller mixing angles to account for the flatter spectrum.

(d) Similar statement as (c) holds for the SMA solution for sterile neutrinos.

Thus our conclusion is that from the statistical point of view all solutions are acceptable since

they all provide a reasonable GOF to the full data set. LMA and LOW-QVO solutions for oscillations into active neutrino seem slightly favoured over SMA solutions for oscillations into active or sterile neutrinos but these last two are not ruled out.

Let's comment now how these conclusions may depend on the specific features of the SSM model and/or the analyzed data. In order to do so we are going to discuss two departures from the previous global analysis:

(a) effect of the uncertainty in the predicted SSM boron flux, and

(b) effect of removing from the analyzed data one of the measured rates.

Concerning (a) in Fig. 14 we show the results of the analysis for active and sterile oscillations when we allow the departure from SSM normalization for the  ${}^8\text{B}$  flux. In doing so we have treated the boron flux as a free parameter that must be fixed by the experiments, in particular by SK. The quality of the different minima is shown in the last line of Table 1. Comparing with the results for fixed SSM  ${}^8\text{B}$  flux we see that allowing free  ${}^8\text{B}$  normalization leads to both an improvement of the quality of the SMA and LMA solutions but the effect is more important for the SMA. The small improvement of the LMA solution is due to the fact that allowing for a free  ${}^8\text{B}$  flux leads to a better simultaneous agreement with Cl and SK measured total rates. The most important effect on the SMA solution arises from the fact that in order to account for a flatter spectrum the SMA solution has shifted to smaller angles, what also implies a larger  ${}^8\text{B}$  flux contribution to both Cl and SK. This can be compensated by the allowance of a lower predicted  ${}^8\text{B}$  flux. Notice also that the LOW solution and QVO solutions which have the best fit very close to the SSM  ${}^8\text{B}$  normalization, the quality of the fit has decreased simply due to the effect of the additional free parameter.

For (b) the situation is more involved. In Fig. 15 we show the analysis for active and sterile oscillations where we have removed the number of events measured by each experiment, SK, Cl and Ga respectively, from the global analysis but always keeping the SK day-night spectra. The

quality of the local minima is showed in Table 2. From the figure and the table we can draw two main conclusions:

- The results for oscillations into active and sterile neutrinos are only significantly different for the LMA and LOW-QVO solutions when both SK and Cl rates are included in the analysis. This is consequence of the larger survival probability for  ${}^8\text{B}$  neutrinos needed to accommodate the measured rate at SK for oscillations into sterile neutrino (due to the absence of the NC contribution) which for large mixing angles lead to a too large contribution to Chlorine rate. On the contrary, if the chlorine experiment is removed from the global analysis both oscillations into active or sterile neutrinos provide equivalently good fits to the data and in particular a large region in both sides of maximal mixing is allowed [17].

- The SMA region is disfavoured in the global analysis due to the spectrum of SK and this result holds independently of the removal of one the measured rates. It is clear by comparing the active SMA and LMA columns of Table 2 that the relative quality of SMA versus LMA worsens when SK or Cl total rates are removed from the analysis. However once both are included (third row), the difference between SMA and LMA descriptions decreases because, as explained before, the worse SMA fit to the SK spectrum is compensated by the better fit to these two rates simultaneously. As a matter of fact, in this case the best solution lies in the LOW region where both rates can be better fitted than for LMA and the spectrum data is better described than for SMA.

Finally let's stress that when the allowed parameter space for solutions of a physics problem consists of a set of isolated regions, the quality of a given solution cannot be inferred from the size of the corresponding region. This fact is nicely illustrated when comparing the SMA solutions for the active and sterile cases shown in Fig. 13. Notice that the SMA region for oscillations into sterile neutrinos is larger than the corresponding one for active neutrinos. This is because it is defined with respect to the global minimum for the sterile oscillation hypothesis (which lies in the SMA region) while the SMA region for the active case is defined with respect to the global minimum

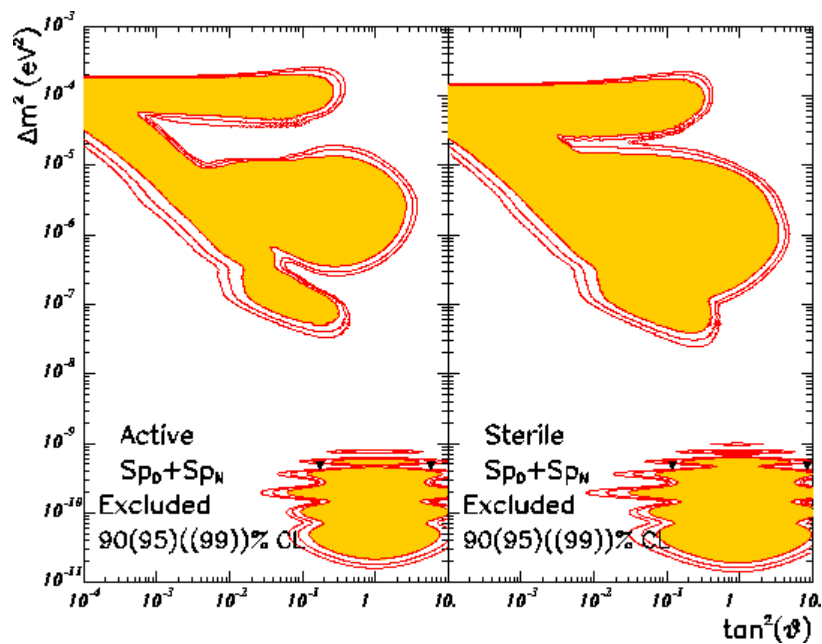


Figure 12. 99 (shadow), 95 and 90 excluded regions from the analysis of the SK measured spectrum at night and at day. The inverted triangle represents the minimum used to define the regions.

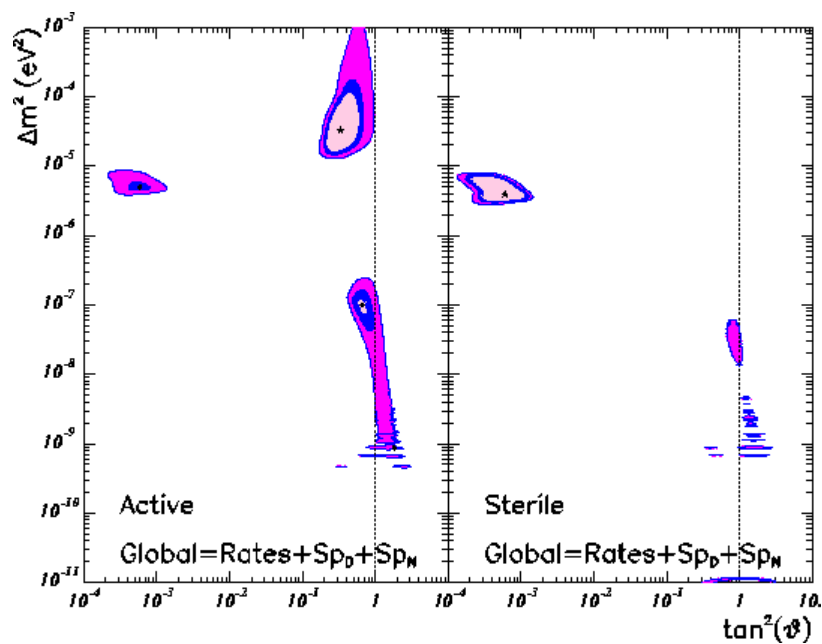


Figure 13. 90, 95 and 99 % CL allowed regions from the global analysis of solar neutrino data including the total measured rates and the SK measured spectrum at day and night. The global minimum is marked with a star while the local minima are denoted with a dot.

Table 1

Best fit points and GOF for the allowed solutions for different combinations of observables.

Observable		Active				Sterile
		SMA	LMA	LOW	VAC-QVO	SMA
Rates	$\Delta m^2/\text{eV}^2$	$5.5 \times 10^{-6}$	$1.9 \times 10^{-5}$	$9.2 \times 10^{-8}$	$9.7 \times 10^{-11}$	$4.1 \times 10^{-6}$
	$\tan^2 \theta$	0.0015	0.3	0.65	0.51 (1.94)	0.0015
	Prob (%)	50 %	8 %	0.5 %	2 %	19 %
Rates +Zenith	$\Delta m^2/\text{eV}^2$	$5.6 \times 10^{-6}$	$5.2 \times 10^{-5}$	$7.9 \times 10^{-8}$	$9.7 \times 10^{-11}$	$4.1 \times 10^{-6}$
	$\tan^2 \theta$	0.0012	0.35	0.69	0.51 (1.94)	0.0015
Rates +Spectrum	$\Delta m^2/\text{eV}^2$	$5.0 \times 10^{-6}$	$2.1 \times 10^{-5}$	$9. \times 10^{-8}$	$8.4 \times 10^{-10}$	$3.9 \times 10^{-6}$
	$\tan^2 \theta$	0.00075	0.32	0.67	1.7 (QVO)	0.00069
Rates +Spec <sub>D</sub> +Spec <sub>N</sub>	$\Delta m^2/\text{eV}^2$	$5.0 \times 10^{-6}$	$3.2 \times 10^{-5}$	$1. \times 10^{-7}$	$8.6 \times 10^{-10}$	$3.9 \times 10^{-6}$
	$\tan^2 \theta$	0.00058	0.33	0.67	1.5 (QVO)	0.0006
	Prob (%)	34 %	59 %	40 %	29 %	30%
Rates +Spec <sub>D</sub> +Spec <sub>N</sub> free $^8\text{B}$	$\Delta m^2/\text{eV}^2$	$4.9 \times 10^{-6}$	$3.0 \times 10^{-5}$	$9.7 \times 10^{-8}$	$8.4 \times 10^{-10}$	$3.9 \times 10^{-6}$
	$\tan^2 \theta$	0.00046	0.26	0.67	1.7 (QVO)	0.00053
	Prob (%)	51 %	65 %	36 %	27 %	42%

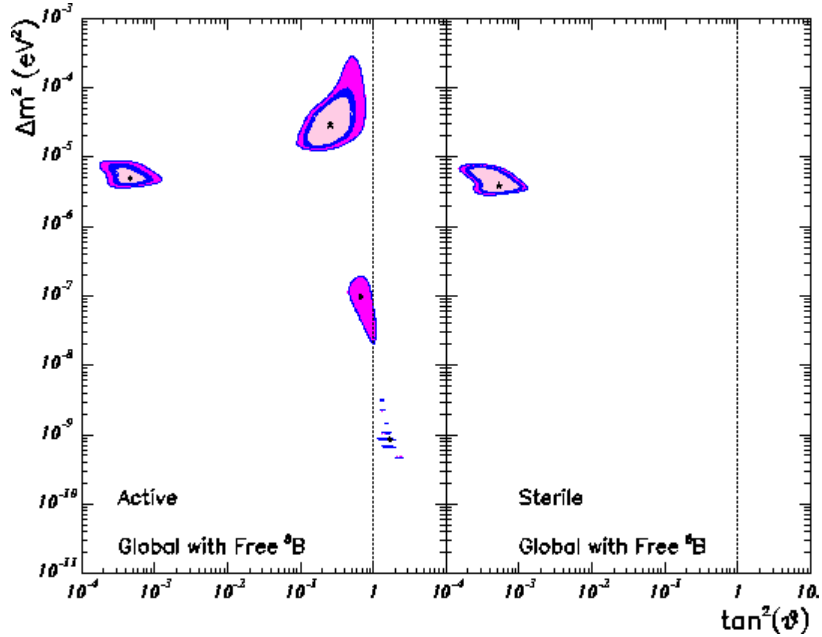


Figure 14. 90, 95 and 99 % CL allowed regions from the global analysis of solar neutrino data taking the boron flux as a free parameter. The global minimum is marked with a star while the local minima are denoted with a dot.

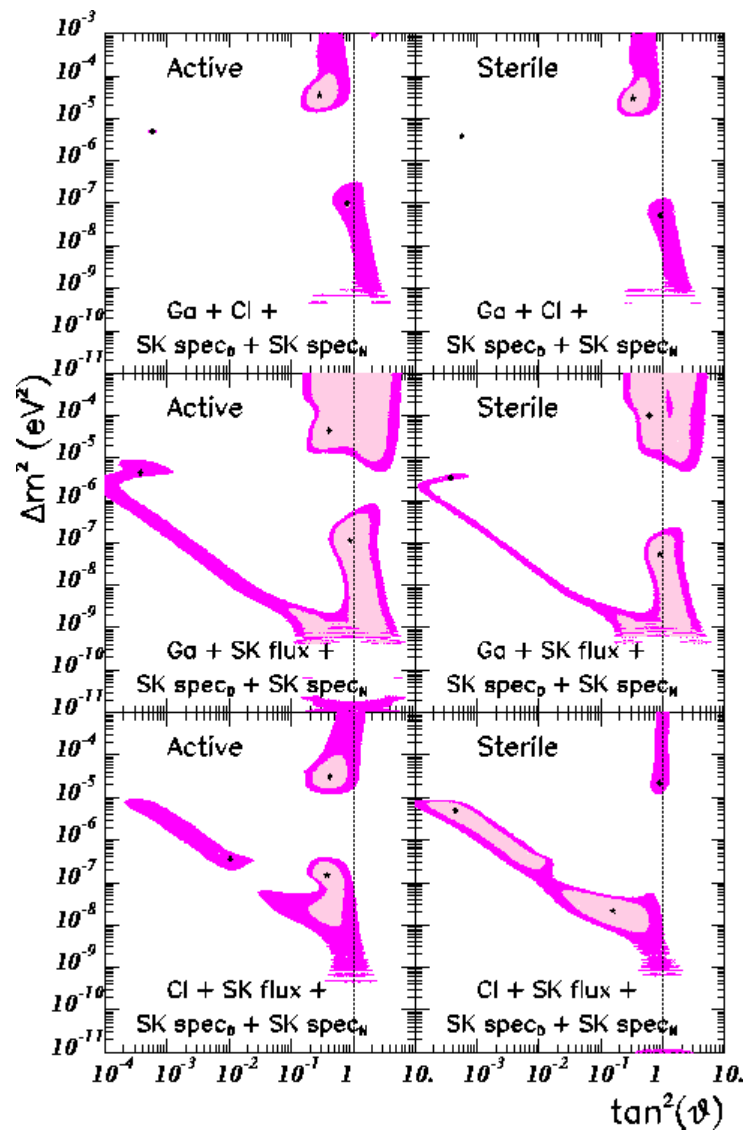


Figure 15. 90 and 99 % CL allowed regions from the global analysis of solar neutrino data where one the fluxes is removed from the data to analyze( SK, Cl and Ga respectively). The global minimum is marked with a star while the local minima are denoted with a dot.

Table 2

$\chi_{min}^2$  and GOF in the regions of SMA, LMA and LOW for the global analysis when one of the fluxes is removed from the data (35 dof).

Observable		Active			Sterile		
		SMA	LMA	LOW	SMA	LMA	LOW
Rates (Ga + Cl) +Spec <sub>D</sub> +Spec <sub>N</sub>	$\chi_{min}$	38.9	29.8	34.3	39.2	29.6	34.3
	Prob (%)	30 %	72 %	50 %	29 %	73 %	50 %
Rates (Ga + SK) +Spec <sub>D</sub> +Spec <sub>N</sub>	$\chi_{min}$	38.1	30.5	30.4	37.2	31.4	29.4
	Prob (%)	33 %	69 %	69 %	37 %	64 %	73 %
Rates (Cl + SK) +Spec <sub>D</sub> +Spec <sub>N</sub>	$\chi_{min}$	38.0	33.0	31.3	39.7	45.7	37.8
	Prob (%)	33 %	56 %	65 %	27 %	12 %	34 %

for that scenario which lies in the LMA. However when looking at the GOF of these two solutions we find that the SMA solution for active case provides a better description of the data than the sterile one despite its region is smaller. In order to put the two scenarios, active and sterile in the same footing we must embed them into a common framework as we describe in the next section.

#### 4. Four–Neutrino Oscillations

In this section we present a brief update of the analysis performed in Ref. [22]. We refer to this publication for further details on the as well as for the relevant references. Here we simply summarize the main ingredients.

Together with the results from the solar neutrino experiments we have two more evidences pointing out towards the existence of neutrino masses and mixing: the atmospheric neutrino data and the LSND results. All these experimental results can be accommodated in a single neutrino oscillation framework only if there are at least three different scales of neutrino mass-squared differences. The simplest case of three independent mass-squared differences requires the existence of a light sterile neutrino, *i.e.* one whose interaction with standard model particles is much weaker than the SM weak interaction, so it does not affect the invisible Z decay width, precisely measured at LEP.

In four-neutrino schemes the flavor neutrino fields  $\nu_{\alpha L}$  ( $\alpha = e, s, \mu, \tau$ ) are related to the fields

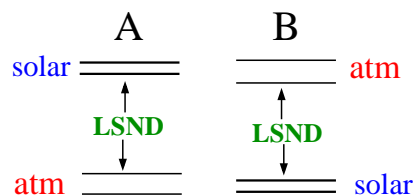
$\nu_{kL}$  of neutrinos with masses  $m_k$  by the relation

$$\nu_{\alpha L} = \sum_{k=1}^4 U_{\alpha k} \nu_{kL} \quad (\alpha = e, s, \mu, \tau), \quad (13)$$

where  $U$  is a  $4 \times 4$  unitary mixing matrix, which contains, in general 6 mixing angles (we neglect here the CP phases).

Existing bounds from negative searches for neutrino oscillations performed at collider as well as reactor experiments impose severe constrains on the possible mass hierarchies as well as mixing structures for the four–neutrino scenario. In particular they imply:

(a) Only two four-neutrino schemes can accommodate the results of all neutrino oscillation experiments. In both these mass spectra



there are two pairs of close masses separated by a gap of about 1 eV which gives the mass-squared difference  $\Delta m_{SBL}^2 = \Delta m_{41}^2$  responsible for the short-baseline (SBL) oscillations observed in the LSND experiment (we use the common notation  $\Delta m_{kj}^2 \equiv m_k^2 - m_j^2$ ). We have ordered the masses in such a way that in both schemes  $\Delta m_{sun}^2 = \Delta m_{21}^2$  produces solar neutrino oscillations and  $\Delta m_{atm}^2 = \Delta m_{43}^2$  is responsible for atmospheric neutrino oscillations.

(b) In the study of solar neutrino oscillations only four mixing angles are relevant and the  $U$  matrix can be written as

$$U = U_{34} U_{24} U_{23} U_{12}. \quad (14)$$

where  $\vartheta_{12}$ ,  $\vartheta_{23}$ ,  $\vartheta_{24}$ ,  $\vartheta_{34}$  are four mixing angles and we will define  $c_{ij} \equiv \cos \vartheta_{ij}$  and  $s_{ij} \equiv \sin \vartheta_{ij}$ .

Since solar neutrino oscillations are generated by the mass-square difference between  $\nu_2$  and  $\nu_1$ , it is clear from Eq. (14) that the survival of solar  $\nu_e$ 's mainly depends on the mixing angle  $\vartheta_{12}$ , whereas the mixing angles  $\vartheta_{23}$  and  $\vartheta_{24}$  determine the relative amount of transitions into sterile  $\nu_s$  or active  $\nu_\mu$  and  $\nu_\tau$ . Let us remind the reader that  $\nu_\mu$  and  $\nu_\tau$  cannot be distinguished in solar neutrino experiments, because their matter potential and their interaction in the detectors are equal, due only to NC weak interactions. The active/sterile ratio and solar neutrino oscillations in general do not depend on the mixing angle  $\vartheta_{34}$ , that contribute only to the different mixings of  $\nu_\mu$  and  $\nu_\tau$ , and depends on the mixing angles  $\vartheta_{23}$   $\vartheta_{24}$  only through the combination  $\cos \vartheta_{23} \cos \vartheta_{24}$ .

Therefore, the oscillations of solar neutrinos depend only on  $\vartheta_{12}$  and the product  $\cos \vartheta_{23} \cos \vartheta_{24}$ . If  $\cos \vartheta_{23} \cos \vartheta_{24} \neq 1$ , solar  $\nu_e$ 's can transform in the linear combination  $\nu_a$  of active  $\nu_\mu$  and  $\nu_\tau$ . We distinguish the following limiting cases:

- $\cos \vartheta_{23} \cos \vartheta_{24} = 0$  corresponding to the limit of pure two-generation  $\nu_e \rightarrow \nu_a$  transitions.
- $\cos \vartheta_{23} \cos \vartheta_{24} = 1$  for which we have the limit of pure two-generation  $\nu_e \rightarrow \nu_s$  transitions.

In the general case of simultaneous  $\nu_e \rightarrow \nu_s$  and  $\nu_e \rightarrow \nu_a$  oscillations the corresponding probabilities are given by

$$P_{\nu_e \rightarrow \nu_s} = c_{23}^2 c_{24}^2 (1 - P_{\nu_e \rightarrow \nu_e}), \quad (15)$$

$$P_{\nu_e \rightarrow \nu_a} = (1 - c_{23}^2 c_{24}^2) (1 - P_{\nu_e \rightarrow \nu_e}). \quad (16)$$

where  $P_{\nu_e \rightarrow \nu_e}$  takes the standard two-neutrino oscillation form (3) for  $\Delta m_{21}^2$  and  $\theta_{12}$  but computed for the modified matter potential

$$A \equiv A_{CC} + c_{23}^2 c_{24}^2 A_{NC}. \quad (17)$$

Thus the analysis of the solar neutrino data in the four-neutrino mixing schemes it is equivalent to the two-neutrino analysis but taking into account that the parameter space is now three-dimensional ( $\Delta m_{21}^2, \tan^2 \vartheta_{12}, \cos^2 \vartheta_{23} \cos^2 \vartheta_{24}$ ).

We first present the results of the allowed regions in the three-parameter space for the global combination of observables. In building these regions, for a given set of observables, we compute for any point in the parameter space of four-neutrino oscillations the expected values of the observables and with those and the corresponding uncertainties we construct the function  $\chi^2(\Delta m_{21}^2, \vartheta_{12}, c_{23}^2 c_{24}^2)$ . We find its minimum in the full three-dimensional space. The allowed regions for a given CL are then defined as the set of points satisfying the condition

$\chi^2(\Delta m_{21}^2, \vartheta_{12}, c_{23}^2 c_{24}^2) - \chi_{min}^2 \leq \Delta \chi^2(\text{CL}, 3 \text{ dof})$  where, for instance,  $\Delta \chi^2(\text{CL}, 3 \text{ dof}) = 6.25, 7.83,$  and  $11.36$  for  $\text{CL} = 90, 95,$  and  $99\%$  respectively. In Figs. 16 we plot the sections of such volume in the plane ( $\Delta m_{21}^2, \tan^2(\vartheta_{12})$ ) for different values of  $c_{23}^2 c_{24}^2$ . The global minimum used in the construction of the regions lies in the LMA region and for pure active oscillations value of  $c_{23}^2 c_{24}^2 = 0$ .

As seen in Fig. 16 the SMA region is always a valid solution for any value of  $c_{23}^2 c_{24}^2$ . This is expected as in the two-neutrino oscillation picture this solution holds both for pure active-active and pure active-sterile oscillations. Notice, however, that the statistical analysis is different: in the two-neutrino picture the pure active-active and active-sterile cases are analyzed separately, whereas in the four-neutrino picture they are taken into account simultaneously in a consistent scheme. We see that in this ‘‘unified’’ framework, since the GOF of the SMA solution for pure sterile oscillations is worse than for SMA pure active oscillations (as discussed in the previous section), the corresponding allowed region is smaller as they are now defined with respect to a common minimum.

On the other hand, the LMA, LOW and QVO solutions disappear for increasing values of the mixing  $c_{23}^2 c_{24}^2$ . In Fig. 17 we show the the values of  $\Delta \chi^2$  (with respect to the global minimum) for the different solutions as a function of  $c_{23}^2 c_{24}^2$ . From this figure we can read the limiting values of  $c_{23}^2 c_{24}^2$  for which a given solution is allowed in a given CL. We list some of this limits in Table 3. We find that at 95% CL the LMA is allowed for maximal active-sterile mixing  $c_{23}^2 c_{24}^2 = 0.5$  while at 99% CL all solutions are possible for this max-

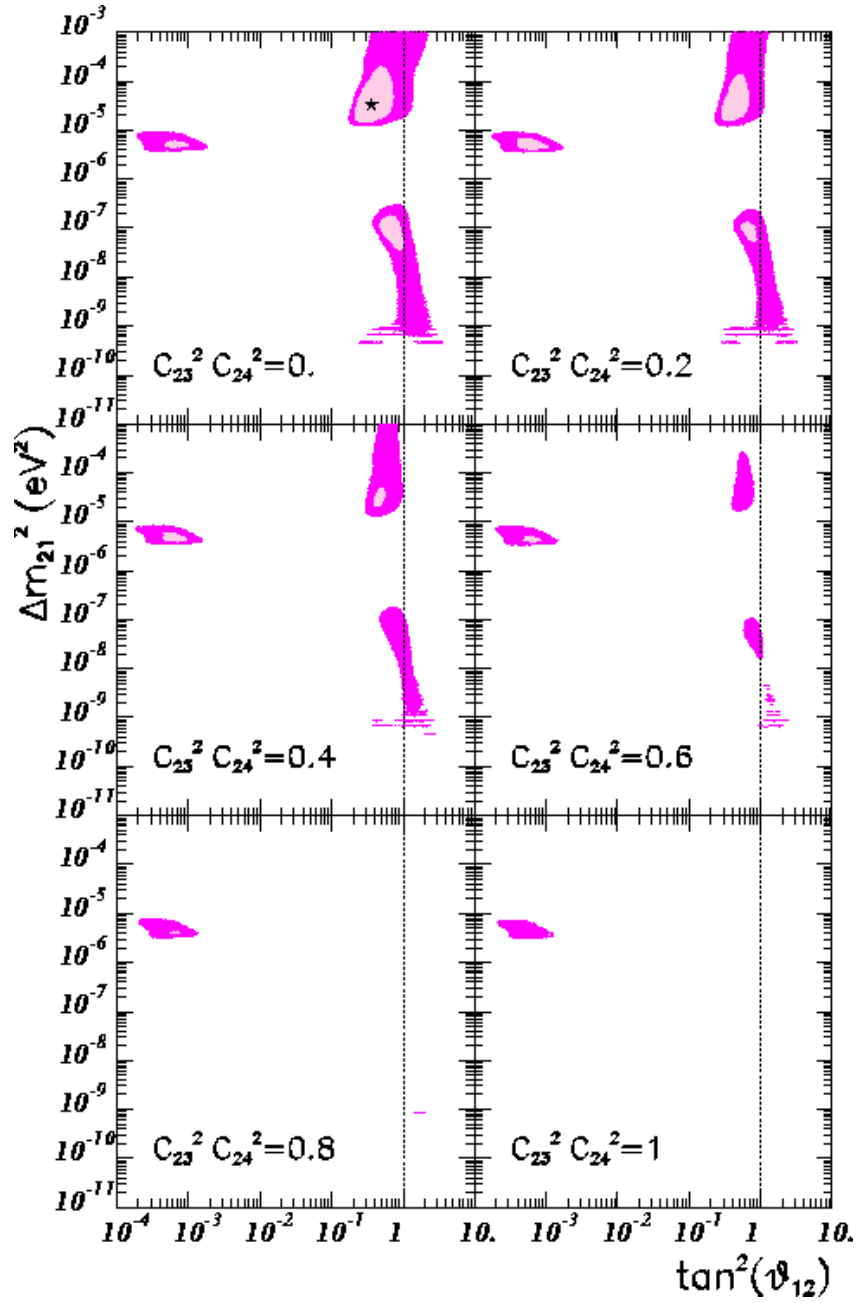


Figure 16. Results of the global analysis for the allowed regions in  $\Delta m_{21}^2$  and  $\tan^2 \vartheta_{12}$  for the four-neutrino oscillations. The different panels represent the allowed regions at 99% (darker) and 90% CL (lighter) obtained as sections for fixed values of the mixing angles  $c_{23}^2 c_{24}^2$  of the three-dimensional volume. The best-fit point in the three parameter space is plotted as a star.



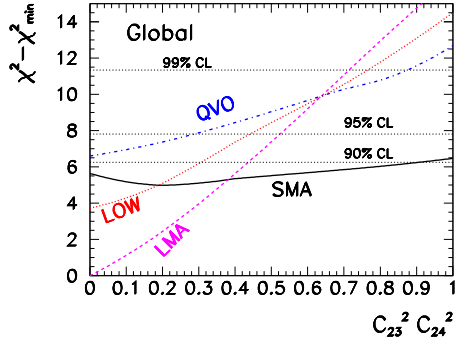


Figure 17.  $\Delta\chi^2$  as a function of the mixing parameter  $c_{23}^2 c_{24}^2$  for the different solutions SMA (full line), LMA (dashed), LOW (dotted) and QVO (dot-dashed) from the global analysis of the rates and the day-night spectrum data. The dotted horizontal lines correspond to the 90%, 95%, 99% CL.

Table 3  
Maximum allowed value of  $\cos^2_{23} \cos^2_{24}$  at 90%, 95%, and 99% CL for the different solutions to the solar neutrino problem.

CL	SMA	LMA	LOW	QVO
90	0.9	0.44	0.3	forbidden
95	all	0.53	0.44	0.28
99	all	0.72	0.77	0.88

imal mixing case.

Other authors have recently performed fits of the atmospheric neutrino data in the framework of the two four-neutrino schemes A and B [23]. We expect that in the future a combined fit of solar and atmospheric neutrino data will allow to constraint further the mixing of four neutrinos.

## 5. Summary and Conclusions

We have studied the status of the solutions of the solar neutrino problem in terms of oscillations of  $\nu_e$  into active or sterile neutrinos in the framework of two-neutrino and four-neutrino mixing, after a global analysis of the full data set corresponding to the latest SK data on the total

event rate, their day-night dependence and the recoil electron energy spectrum, together with the data from Chlorine and Gallium experiments presented at the  $\nu$ -2000 conference. In particular we have shown the possible solutions in the full parameter space for oscillations including both MSW and vacuum, as well as QVO and matter effects for mixing angles in the second octant

Our main conclusions from the two-neutrino oscillation analysis are the following:

- From the statistical point of view, all solutions for oscillations into active neutrinos: LMA, LOW, SMA, QVO solutions are acceptable since they all provide a reasonable GOF to the full data set.
- The same holds for the SMA solution, which is the best possible solution for oscillations into sterile neutrinos.
- LMA and LOW-QVO solutions for oscillations into active neutrinos seem slightly favoured over SMA solutions for oscillations into active or sterile neutrinos due to the flatter spectrum of SK.
- Oscillations into sterile neutrino provide a slightly worse fit.
- When allowing for a free  $^8\text{B}$  normalization weakens the conclusion (c).
- Removing the total rate measured at Chlorine or SK from the analysis weakens conclusion (d) and straightens conclusion (c).

For the analysis of four-neutrino oscillations, which allows for oscillations into a state which is a combination of active and sterile neutrino, we find that the SMA region is always a valid solution while the LMA, LOW and QVO solutions disappear for increasing values of the additional mixing  $c_{23}^2 c_{24}^2$ . However we find that at 95% CL the LMA is still allowed for maximal active-sterile mixing  $c_{23}^2 c_{24}^2 = 0.5$  while at 99% CL all solutions are possible for this maximal mixing case.

## REFERENCES

- J. N. Bahcall, S. Basu and M. H. Pinsonneault, Phys. Lett. **B433**, 1 (1998).

2. B. T. Cleveland *et al.*, *Astrophys. J.* **496**, 505 (1998); R. Davis, *Prog. Part. Nucl. Phys.* **32**, 13 (1994).
3. SAGE Collaboration, J. N. Abdurashitov *et al.*, *Phys. Rev.* **C60**, 055801 (1999); Talk by V. Gavrin at Neutrino 2000, Sudbury, Canada, June 2000 (<http://nu2000.sno.laurentian.ca>).
4. GALLEX Collaboration, W. Hampel *et al.*, *Phys. Lett.* **B447**, 127 (1999).
5. Talk by E. Belloti at Neutrino 2000, Sudbury, Canada, June 2000 (<http://nu2000.sno.laurentian.ca>).
6. Super-Kamiokande Collaboration, Y. Fukuda *et al.*, *Phys. Rev. Lett.* **81**, 1158 (1998); Erratum **81**, 4279 (1998); **82**, 1810 (1999); **82**, 2430 (1999); Y. Suzuki, *Nucl. Phys. B (Proc. Suppl.)* **77**, 35 (1999).
7. Talk by Y. Suzuki at Neutrino 2000, Sudbury, Canada, June 2000 (<http://nu2000.sno.laurentian.ca>).
8. A. B. McDonald, *Nucl. Phys. B (Proc. Suppl.)* **77**, 43 (1999); SNO Collaboration, *Physics in Canada* **48**, 112 (1992); SNO Collaboration, *nucl-ex/9910016*.
9. V.N. Gribov and B.M. Pontecorvo, *Phys. Lett.* **28B**, 493 (1969); V. Barger, K. Whisnant, R.J.N. Phillips, *Phys. Rev.* **D24**, 538 (1981); S.L. Glashow and L.M. Krauss, *Phys. Lett.* **190B**, 199 (1987).
10. S.P. Mikheyev and A.Yu. Smirnov, *Sov. Jour. Nucl. Phys.* **42**, 913 (1985); L. Wolfenstein, *Phys. Rev.* **D17**, 2369 (1978).
11. S. T. Petcov, *Phys. Lett.* **B200**, 373 (1988); P. I. Krastev and S. T. Petcov, *Phys. Lett.* **B207**, 64 (1988).
12. <http://www.sns.ias.edu/~jnb/SNdata/Export/BP2000>; J. N. Bahcall, S. Basu and M. H. Pinsonneault, *Astrophys. J.* **529**, 1084 (2000).
13. A. M. Dziewonski and D. L. Anderson, *Phys. Earth Planet. Inter.* **25**, 297 (1981).
14. J. Pantaleone, *Phys. Lett.* **B251**, 618 (1990); S. Pakvasa and J. Pantaleone, *Phys. Rev. Lett.* **65**, 2479 (1990)
15. A. Friedland, *Phys. Rev. Lett.* **85**, 936 (2000).
16. G. L. Fogli, E. Lisi, D. Montanino and A. Palazzo, *hep-ph/0005261*; A.M. Gago, H. Nunokawa, R. Zukanovich Funchal, *hep-ph/0007270*.
17. M.C. Gonzalez-Garcia, C. Peña-Garay, Y. Nir, A. Yu. Smirnov, *hep-ph/00007227*.
18. A. de Gouvea, A. Friedland and H. Murayama, *hep-ph/0002064*.
19. M. C. Gonzalez-Garcia, C. Peña-Garay, *Phys. Rev.* **D62**, 031301 (2000).
20. G. L. Fogli, E. Lisi, A. Maronne and G. Scioscia, *Phys. Rev.* **D59**, 033001 (1999).
21. M. C. Gonzalez-Garcia, P. C. de Holanda, C. Peña-Garay, J. W. F. Valle, *Nucl. Phys.* **B573**, 3 (2000).
22. C. Giunti, M. C. Gonzalez-Garcia, C. Peña-Garay, *Phys. Rev.* **D62**, 013005 (2000).
23. O. Yasuda, *hep-ph/0006319*; E. Lisi, Talk presented at Neutrino 2000, Sudbury, Canada, June 2000 (<http://nu2000.sno.laurentian.ca>).